J. Fluid Mech. (2006), *vol.* 563, *pp.* 283–292.
doi:10.1017/S0022112006001662 Printed in the United Kingdom

Fall and rise of a viscoelastic filament

By ANSHUMAN ROY[1], L. MAHADEVAN[2] AND JEAN-LUC THIFFEAULT[3]

[1]Department of Chemical Engineering, University of Michigan, Ann Arbor, MI 48109, USA
[2]Division of Engineering & Applied Sciences, Harvard University, Cambridge, MA 02138, USA
[3]Department of Mathematics, Imperial College London, SW7 2AZ, UK

(Received 10 January 2006 and in revised form 28 June 2006)

When a viscoelastic fluid blob is stretched out into a thin horizontal filament, it sags and falls gradually under its own weight, forming a catenary-like structure that evolves dynamically. If the ends are brought together rapidly after stretching, the falling filament tends to straighten by rising. These two effects are strongly influenced by the elasticity of the fluid and yield qualitatively different behaviours from the case of a purely viscous filament analysed previously (Teichman & Mahadevan, *J. Fluid Mech.* vol. 478, 2003, p. 71). Starting from the bulk equations for the motion of a viscoelastic fluid, we derive a simplified equation for the dynamics of a viscoelastic filament and analyse this equation in some simple settings to explain our observations.

1. Introduction

Fluid sheets and filaments, which are ubiquitous in science and technology, are marked by a slender aspect ratio. This geometric separation of length scales leads to a separation of time scales that is at the heart of a range of unusual behaviour arising from the confluence of geometry and physics in these objects. While this interplay has been the subject of much research in the context of simple Newtonian fluids, only recently have analogous questions been asked for complex fluids, such as those encountered commonly in the kitchen when an egg is broken, in the bathroom when shampoo is squirted from a bottle, and in a host of applications such as rheometry and fibre processing of polymer melts and solutions (McKinley & Sridhar 2002; Denn 2004). However, much of this work has been focused on the one-dimensional dynamics of stretching and the accompanying thinning (Keiller 1992; Entov & Hinch 1997; Olagunju 1999). To understand the behaviour of viscoelastic filaments free to deform in space, we focus here on a thin filament of viscoelastic fluid that can sag under its own weight – the viscoelastic catenary – motivated by recent studies of a viscous catenary of a Newtonian fluid (Teichman & Mahadevan 2003).

To make the filament, we used a 'Boger' fluid (see Larson 1999) composed of 0.025 % w/w Polystyrene of molecular weight 1.877×10^6 dissolved in styrene oil. The relaxation time of this fluid, λ, is ~ 4 s and its zero-shear viscosity, η_0, is ~ 50 Pa s (50 000 times that of water).

Figure 1 shows a filament of such a fluid, made by stretching a blob horizontally between two supporting rods and allowing it to evolve under the influence of gravity. The initial stretching of the blob leads to the stretching of polymer molecules inside the fluid, which then imparts an elastic stress to the filament. As this stress relaxes, the filament initially demonstrates a similar range of motions to the purely viscous

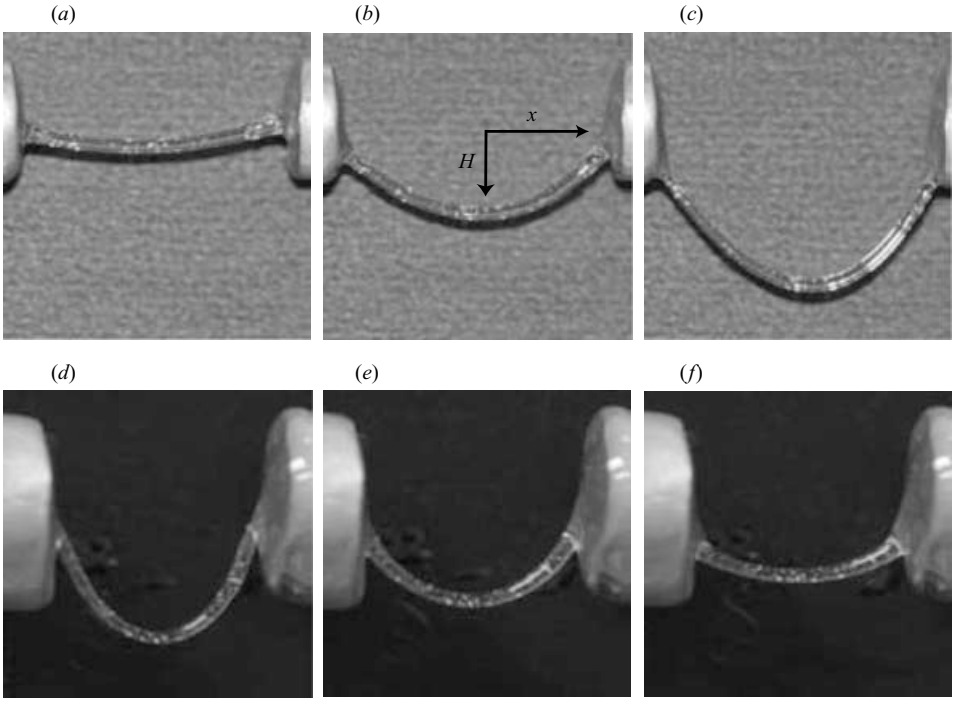

FIGURE 1. Snapshots of a falling viscoelastic filament at different instants of time (t) in s (a) $t = 0^+$, (b) $t = 4$, (c) $t = 8$, and of the rising filament in a separate experiment where the ends of the filament are rapidly brought closer together after initial stretching, (d) $t = 0^+$, (e) $t = 0.75$, (f) $t = 1.75$. The notation that follows in the derivation is shown in (b). The solid anchors on the sides have a cylindrical cross-section of diameter 1.2 cm. In this case, the fluid is a mixture of Polystyrene (MW 1.877×10^6) in styrene oil – a Boger fluid. The zero shear viscosity is approximately 50 Pa s and there is no shear thinning for the shear rates under consideration.

filament (Teichman & Mahadevan 2003) – bending at short times scales and stretching at long time scales (figure 1*a–c*). However, as the filament stretches even more, the elastic stress imparted by the polymer molecules leads to a slowing down of the sagging at long time scales, an effect that is not present in the purely viscous case. If, after the initial stretching, the supporting ends of the filament are brought together quickly, the filament rises. Although the elastic stresses in the filament favour rapid axial contraction, the combined effects of viscosity and the slender geometry of the filament prevent this from happening; instead the excess length of the filament between the supporting ends is accommodated by rapid sagging (figure 1*d*). Then the unbalanced elastic stresses acting along the curved filament cause the viscoelastic filament to rise and straighten, all the while opposing gravity (figure 1*e*, *f*). As the elastic stresses relax, this process eventually slows down over a time scale comparable to the relaxation time of the fluid, ~ 4 s.

To understand this behaviour and compare and contrast it with that of the viscous catenary (Teichman & Mahadevan 2003), we use a perturbation approach to derive the equation governing the motion of the centreline of the fluid filament following Buckmaster, Nachman & Ting (1975), Entov & Yarin (1984), Howell (1996) and Ribe (2001) for the viscous case, and use the resulting dynamical equation to provide a simple quantitative theory for the two phenomena described above.

2. Equations of motion and asymptotic analysis

For simplicity, we start with a consideration of the dynamics of a thin viscoelastic sheet, and then generalize the results appropriately to arrive at a dynamical equation of motion for a viscoelastic filament. We assume that the sheet is made of an incompressible viscoelastic fluid, and is supported between two walls at a distance length L apart. We further assume that the motion of the sheet is confined to the (x, y)-plane and that the initial thickness of the sheet is $h = d$. The governing equations of mass and momentum conservation are then

$$\nabla \cdot \boldsymbol{u} = 0, \tag{2.1}$$

$$\rho(\boldsymbol{u}_t + \boldsymbol{u} \cdot \nabla \boldsymbol{u}) = -\nabla p + \mu \nabla^2 \boldsymbol{u} + \nabla \cdot \boldsymbol{\mathscr{T}} - \rho \boldsymbol{g}, \tag{2.2}$$

where $(\cdot)_t = \partial(\cdot)/\partial t$, $\boldsymbol{u}$ is the fluid velocity, $\boldsymbol{\mathscr{T}}$ is the polymer stress tensor, ρ the fluid density, p its pressure, μ its zero-shear viscosity, and $\boldsymbol{g}$ the gravity vector acting in the negative y-direction. For simplicity, we use a minimal correctly invariant constitutive equation for a viscoelastic fluid that generalizes the Maxwell model valid for small deformations, the Oldroyd-B model (see Oldroyd 1950; Larson 1988),

$$\boldsymbol{\mathscr{T}}_t + \boldsymbol{u} \cdot \nabla \boldsymbol{\mathscr{T}} - (\nabla \boldsymbol{u})^T \cdot \boldsymbol{\mathscr{T}} - \boldsymbol{\mathscr{T}} \cdot (\nabla \boldsymbol{u}) = -\frac{1}{\lambda}(\boldsymbol{\mathscr{T}} - \bar{\mathscr{G}}\boldsymbol{I}), \tag{2.3}$$

where $\bar{\mathscr{G}}$ is the equilibrium polymer stress. This equation describes the evolution of the stress as it is advected and stretched by the flow while it simultaneously tries to relax. The left-hand side of (2.3) is the so-called Oldroyd (upper-convected) derivative of $\boldsymbol{\mathscr{T}}$, while the right-hand side characterizes the tendency of the stress to relax to its equilibrium state $\boldsymbol{\mathscr{T}} = \bar{\mathscr{G}}\boldsymbol{I}$ at a rate $1/\lambda$, where λ is the longest relaxation time of the polymers.

To complete the formulation of the problem, we need to specify some boundary conditions. In addition to the usual kinematic boundary conditions, for large values of the capillary number $\mu U/\gamma$, with γ the interfacial tension, the lateral surfaces $y = H \pm h/2$ are traction-free, so that

$$v = \left(H \pm \tfrac{1}{2}h\right)_t + u\left(H \pm \tfrac{1}{2}h\right)_x, \qquad \boldsymbol{\sigma} \cdot \hat{\boldsymbol{n}} = 0, \tag{2.4a,b}$$

where, $\boldsymbol{\sigma} = -p\boldsymbol{I} + \mu(\nabla \boldsymbol{u} + \nabla \boldsymbol{u}^{\mathrm{T}}) + \boldsymbol{\mathscr{T}}$, is the total stress tensor and $\hat{\boldsymbol{n}}$ is the unit vector in the direction of the outward normal to the surface of the fluid sheet.

We make the above equations dimensionless by scaling all velocities with a characteristic velocity U (determined say by the balance between gravity and viscosity), all lengths with the length of the sheet L, time with L/U, and stress as well as pressure with $\mu U/L$. We also define the Reynolds number $Re = \rho U L/\mu$ characterizing the ratio of inertial to viscous forces, the Weissenberg number $Wi = \lambda U/L$ characterizing the ratio of the internal relaxation time to the externally imposed time, the dimensionless equilibrium stress $\mathscr{G} = \bar{\mathscr{G}}/(\mu U/L)$, and the dimensionless weight $\varpi = \rho g L^2/\mu U$.

The slenderness of the sheet allows us to define a small parameter $\epsilon = h/L \ll 1$, in terms of which we write down an asymptotic expansion for the variables $u, v, H, h, p, \boldsymbol{\mathscr{T}}$. Substituting this expansion into (2.1) and (2.2), solving the equations order by order and using the Fredholm-alternative theorem (see e.g. Hinch 1991), yields an equation of motion for the centreline $H(x, t)$ of the sheet,

$$Re\, H_{tt} + \tfrac{1}{3}d^2\, H_{xxxxt} = [4T H_{xx} + \Psi H_{xx}] + \sigma_x - \varpi, \tag{2.5}$$

where $\sigma = \mathscr{T}_0^{xy}$ is the viscoelastic shear stress, T is the tension in the filament, and $\Psi = \mathscr{T}^{xx} - \mathscr{T}^{yy}$ is the viscoelastic first normal stress difference. The various terms in

(2.5) have simple physical interpretations: the first term on the left is the inertial term present in the equation for the motion of a string, while the second is the viscous bending term that arises from the effects of the solvent, as in the viscous catenary (Teichman & Mahadevan 2003). The first term on the right is the product of the sheet's curvature and tangential stress, which itself has two components – a viscous component that is the same as for the fluid catenary (Teichman & Mahadevan 2003), and a new elastic component. The second term on the right is the spatial derivative of the elastic shear resultant, while the last term is the weight per unit length per unit width of the sheet.

We now consider a sheet of unit initial length (scaled by L) at $t=0$, symmetric about $x=0$, and anchored at its two ends to solid walls at $x=\pm 1/2$, subject to homogeneous extensional flow. Horizontal force balance implies that the tension satisfies $T_x=0$, so that (see the Appendix)

$$T(x,t)=T(t)=\int_0^{1/2}\left(H_x^2\right)_t\,\mathrm{d}x. \tag{2.6}$$

Furthermore, for weak homogeneous extensional flows the normal and shear stresses relax exponentially, with a characteristic decay time set by the Weissenberg number; this is indeed the case even for the case considered here, as the leading-order stress balance shows (see Appendix for details), yielding

$$\Psi=\Psi_0\,\mathrm{e}^{-t/Wi},\quad \sigma=\Psi_0\,H_x\mathrm{e}^{-t/Wi}. \tag{2.7}$$

Equations (2.5)–(2.7) are the governing equations for the shape and stress in the viscoelastic sheet.

The foregoing derivation was for a sheet of infinite extent in the z-direction. For an axisymmetric viscoelastic filament, the equations are almost identical, except that the bending stiffness of a filament is $3\mu\pi d^4/64$ (see Teichman & Mahadevan 2003), and all other prefactors have to be re-interpreted as being per unit cross-sectional area of the filament. When inertia is unimportant ($Re\ll 1$), as here, we can integrate (2.5) once to obtain

$$\frac{\epsilon^3}{32}\,\theta_{xxt}=\epsilon\,\theta\left(\frac{1}{2}\int_0^{1/2}(\theta^2)_t\,\mathrm{d}x+\Lambda_0\,\mathrm{e}^{-t/Wi}\right)-x, \tag{2.8}$$

where $\Lambda_0=\Lambda\Psi_0$ and $\theta=H_x$. Here we have rescaled time using the intrinsic time $6\mu/\rho g d$, the stresses $\sigma=\mathscr{T}^{xy}$ and Ψ using the equilibrium polymer stress $\bar{\mathscr{G}}$, and define $\Lambda_0=\Psi_0\bar{\mathscr{G}}/\rho g d$. Equation (2.8), when complemented with initial and boundary conditions, is identical to that for the weakly nonlinear dynamics of a viscous catenary described and analysed in Teichman & Mahadevan (2003), except for the second term on the right which reflects the effect of a decaying elastic stress.

For the filament shown in figure 1, the diameter $d=0.001\,\mathrm{m}$, length $L=0.023\,\mathrm{m}$, weight $w=0.125\,\mathrm{N\,m^{-1}}$, density $\rho=1026\,\mathrm{kg\,m^{-3}}$ and relaxation time $\lambda=4\,\mathrm{s}$, which results in $\epsilon=0.045$ and $Wi=0.13$. In the analysis that follows, we use $Wi\in[0.001,0.1]$, $\Lambda_0=25$ and $\epsilon=0.02$ in (2.8) to describe the dynamics of a viscoelastic filament. The value of Λ_0 we pick is arbitrary, since we do not have an accurate estimate of its value for the experiments shown in figure 1. We emphasize that here we have limited ourselves to the simplest consistent constitutive model that leads to an embedded stress in the filament due to initial stretching, even though the initial stretching may be fast enough to invalidate the Oldroyd-B model which does not account for the finite extensibility of the polymer.

3. Analysis of filament behaviour

We now use our slender body theory to investigate the falling and rising of a filament and uncover the role of elastic stresses in each case.

3.1. *Fall*

An initially horizontal fluid filament must bend as it sags under its own weight. With the assumption of symmetry about $x=0$, the initial condition is $\theta(x,0)=0$, and boundary conditions are

$$\theta(\pm 1/2, t) = 0,\ H(\pm 1/2, t) = 0. \tag{3.1}$$

Physically, these boundary conditions mean that the ends of the filament are clamped at the points of support, and are the same as used by Teichman & Mahadevan (2003). We solve the integro-differential equation (2.8) with these conditions using a pseudospectral scheme based on Chebyshev polynomials (Trefethen 2000; Teichman & Mahadevan 2003). Figure 2(*a*) shows the results of the evolution of the shape of the viscoelastic catenary at early, intermediate and late times; different curves correspond to snapshots separated by equal intervals of time. We see two characteristic behaviours of the filament: at early times, the filament falls at roughly constant velocity and its shape has two inflection points where the curvature changes sign, while at late times the filament slows down considerably and the inflection points become imperceptible. To understand this behaviour, we note that in the limit $\epsilon \ll 1$ corresponding to a slender filament (2.8) is singular, and thus exhibits different asymptotic regimes. At early times, when the filament is nearly horizontal, θ is nearly zero and the dominant balance is between the viscous bending term on the left side of (2.8) and the filament weight. During this time, the evolution of the viscoelastic filament is practically identical to that of a purely viscous filament, with

$$\frac{\epsilon^3}{32}\,\theta_{xxt} \approx -x, \tag{3.2}$$

so that the analysis is identical to that in Teichman & Mahadevan (2003), yielding

$$H(x,t) = \int_{-1/2}^{x} \theta(x',t)\,\mathrm{d}x' \approx -\tfrac{4}{3}\epsilon^{-3}\,t\left(\tfrac{1}{4}-x^2\right)^2. \tag{3.3}$$

Although the viscous bending–gravity balance is reasonable at early times, it fails at intermediate times when the filament slows down as it starts to stretch. Then stretching and elastic terms become important in the bulk of the filament, where they approximately balance gravity. If $\theta^{(o)}$ refers to the solution in this region,

$$\epsilon\,\theta^{(o)}\left(\frac{1}{2}\int_0^{1/2}\left(\theta^{(o)}\right)_t^2\,\mathrm{d}x + \Lambda_0\,\mathrm{e}^{-t/Wi}\right) \approx x, \qquad x \in \left[0,\ \tfrac{1}{2}-\delta\right]. \tag{3.4}$$

Here δ is the width of the dynamic boundary layer over which there is a transition from the stretching-dominated region to the bending-dominated region to accommodate the clamped boundary condition $\theta(0,t)=0$. Letting $\theta^{(o)}=a(t)x$ in the interior so that $H(x,t)=\frac{1}{2}a(t)(x^2-\frac{1}{4})$, and substituting into (3.4), we obtain

$$a^2\frac{\mathrm{d}a}{\mathrm{d}t} = \frac{24}{\epsilon}\left(1-\epsilon\Lambda_0\,\mathrm{e}^{-t/Wi}a\right). \tag{3.5}$$

In figure 2(*a*), we see that the full numerical solution of (2.8) and (3.1) compares well with the approximate equations (3.2) and (3.5) in the two asymptotic regimes of (2.8) that arise naturally at early and intermediate times.

To understand the evolution of the dynamic boundary layers in the viscoelastic filament, we first note that the size of this layer is determined by the balance

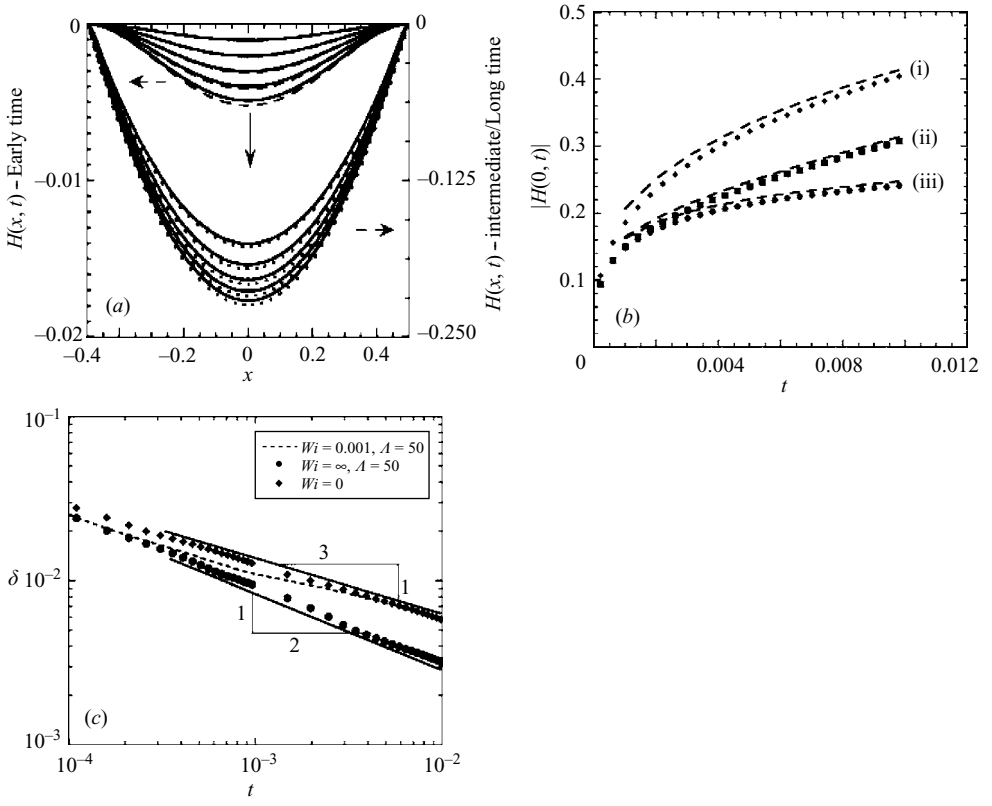

FIGURE 2. (*a*) Early time bending-dominated regime of a viscoelastic filament, and the late time stretching-dominated regime for $\epsilon = 0.02$, $\Lambda_0 = 25$, $Wi = 0.1$. The numerical solution to the complete equation describing the shape of the filament, (2.8), is plotted with solid lines, and the analytical solution to the approximate equation for the bending regime, (3.2), is in long-dashed lines. The numerical solution to the approximate equation, (3.4), is plotted in short-dashed lines. The vertical downward arrow shows the direction of increasing time. (*b*) Maximum displacement of catenary, $|H(0, t)|$, as a function of the scaled time t for $\epsilon = 0.02$ and (i) purely viscous case, (ii) $\Lambda_0 = 25$, $Wi = 0.01$, (iii) $\Lambda_0 = 25$, $Wi = 0.1$. The points and the dashed lines are numerical solutions to (2.8) and (3.4), respectively. (*c*) Width of the viscous boundary layer δ near the supporting walls as a function of time, for values of parameters shown in the legend. For the purely viscous case ($Wi = 0$, diamonds) $\delta \sim \epsilon^{4/3} t^{-1/3}$, while for the purely elastic case ($Wi = \infty$, circles) $\delta \sim \epsilon \Lambda_0^{-1/2} t^{-1/2}$ (see text). For a viscoelastic filament (dashed line), the boundary layer width is dominated by elastic effects at short times and viscous effects at long times.

between the effects of filament bending and filament weight. Equation (2.8) thus yields $\epsilon^3 \theta^{(o)} / \delta^2 t \sim x$. In the viscous limit, when the Weissenberg number $Wi \to 0$, (3.4) gives the interior solution $\theta^{(o)} \sim x t^{1/3} \epsilon^{-1/3}$, so that boundary layer size scales as $\delta \sim \epsilon^{4/3} t^{-1/3}$ (see Teichman & Mahadevan 2003). In the elastic limit, $Wi \to \infty$ and (3.4) yields the stationary solution $\theta^{(o)} \approx x / \epsilon \Lambda_0$. The size of the boundary layer is then $\delta \sim \epsilon \Lambda_0^{-1/2} t^{-1/2}$. In figure 2(*c*), we show the numerically evaluated evolution of the size of the boundary layer for varying Wi; at short times the boundary layer is similar to that in the elastic limit ($Wi \to \infty$), while at long times it is similar to that in the viscous limit ($Wi \to 0$), as expected.

In the intermediate time regime, outside the two dynamic boundary layers near the supports the shape of the filament is very nearly parabolic and determined by a

balance of viscoelastic stretching and gravity. Indeed choosing $H(x,t)=\frac{1}{2}a(t)(x^2-\frac{1}{4})$ and substituing this ansatz into (2.8) we find that the centre of the filament follows the law $H(0,t) \equiv H_c(t)=a(t)/8$. In figure 2(*b*) we show $|H_c(t)|$ for $\Lambda_0=25$ and different values of Wi. The embedded elastic stress within the filament, i.e. $\Lambda_0>0$, slows down its sagging. For $Wi\to\infty$, (3.5) predicts that the filament stops falling when $H_c(t\to\infty)=1/(8\Lambda_0\epsilon)$, while for $Wi\to 0$ we recover the case of a purely viscous filament (Teichman & Mahadevan 2003). The figure also shows the slowdown of the filament with increasing Wi due to the additional resistance offered by the elastic stresses. Smaller values of Wi result in faster relaxation of the elastic stresses and at long times the behaviour is similar to that of the viscous catenary with $a\sim\epsilon^{-1/3}t^{1/3}$.

3.2. *Rise*

When a filament is stretched out rapidly from a blob, the stretching of the polymers leads to an embedded elastic stress. If the supporting ends are brought together quickly the resulting geometrically induced sagging can be reversed by this elastic stress, leading to the rising of the filament.

To quantify this, we first consider the extreme case of a filament that is curved, say parabolically at time $t=0$ with $\Lambda_0>0$, $Wi\to\infty$, and $a(0)\gg 1/(\Lambda_0\epsilon)$. Then from (3.5), $\mathrm{d}a/\mathrm{d}t<0$ and the filament rises against its own weight until $\mathrm{d}a/\mathrm{d}t=0$, i.e. when $a=1/(\Lambda_0\epsilon)$. For a fluid with a finite relaxation time, and therefore a finite Wi, the embedded viscoelastic stress decays with time and the filament slows down as it rises. More generally, the *rising criterion* at $t=0$, is defined by the condition

$$\epsilon\,\Lambda_0 H_c > 1/8 \tag{3.6}$$

where $H_c=a/8$. As the filament straightens, it re-enters the viscous bending-dominated regime. Since both the elastic and viscous resistance to stretching and contraction are proportional to θ, it is clear that in the absence of inertia the filament can never rise to a perfectly horizontal state starting from a sagged state. On the other hand, inertial effects can cause the filament to rebound past the horizontal, an effect that can sometimes be seen with a stretched piece of chewing gum, but that we do not consider here. In figure 3(*a*) we show the rising of an initially curved filament and see that there is excellent agreement between the numerical solutions to the full equation (2.8) and the approximate equation (3.4).

We confirm the rising criterion by solving (2.8) with an initial condition corresponding to a falling filament, $H(x,0)=H_c(1-x^2/4)$. In figure 3(*b*), we plot the maximum rising displacement $H(0,t)-H(0,0)=H(0,t)-H_c$ of the filament, and look at the effect of varying Wi for given initial stress Λ_0. For $Wi=0.1$, the filament rises fast initially and attains a nearly constant shape, while for $Wi=0.001$, the elastic stress decays too rapidly (by $1/e$ of its initial value in $t\sim Wi$ for this case), so that it falls further instead of rising. The rising criterion (3.6) is met in each of the cases at $t=0$, since for $\epsilon=0.02$, $\Lambda_0=25$ and $H_c=0.35$, $\epsilon\Lambda_0H_c=7/40>1/8$.

4. Discussion

Our asymptotic analysis of the flow of a viscoelastic fluid in slender geometry yielded a pair of simple evolution equations for the shape of and the stress in a filament. These equations have a transparent physical interpretation that builds on and complements earlier work on the purely viscous case (Teichman & Mahadevan 2003). In particular, we see that the effect of elastic normal stresses suffices to explain both the falling and rising behaviour of a viscoelastic filament in the limit of moderate deviations from the horizontal. Although the physical values in the experiment are not

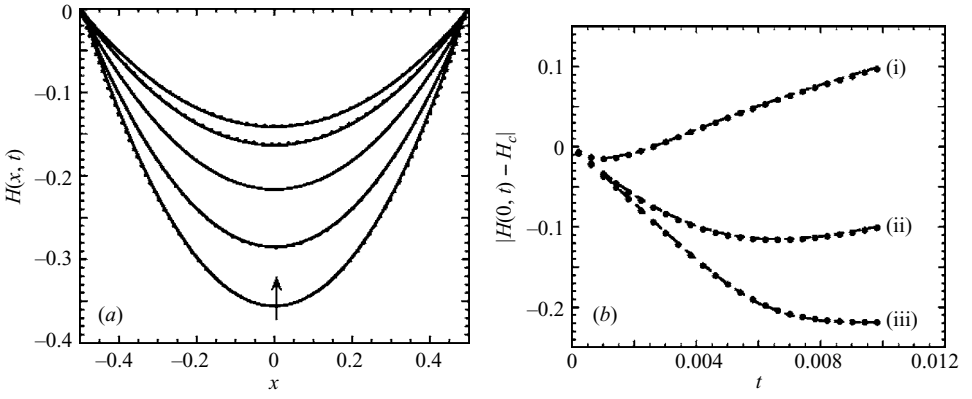

FIGURE 3. (*a*) Rising of an initially curved filament obtained by solving (2.8) with boundary conditions $\theta(\pm 1/2, t) = 0$; the lowermost curve shows the position of the filament at $t = 0^-$, i.e. with the initial condition set numerically by allowing the filament to fall so that $H_c = 0.355$. This shape is very well approximated by $H(x, 0) \sim 1.42(x^2 - \frac{1}{4})$. The vertical upward arrow shows the direction of increasing time. The catenary rises due to the embedded elastic stress, and is opposed by the viscous stretching term which now acts in the direction of gravity ($\epsilon = 0.02$, $\Lambda_0 = 25$, $Wi = 0.1$). The barely visible dashed line is the solution to the approximate equation (3.4), showing excellent agreement with the complete solution. (*b*) Maximum rising displacement of catenary, $|H(0, t) - H_c|$, against scaled time t for $\epsilon = 0.02$ and $\Lambda_0 = 25$, (i) $Wi = 0.001$, (ii) $Wi = 0.01$, (iii) $Wi = 0.1$. The circles corresponds to the numerical solution to (2.8), while the dashed line shows the numerical solution to the approximate equation (3.4).

fully compatible with the scalings assumed in the derivation of (2.5), the qualitative behaviour of the filament agrees well with the conclusions derived from it. This is perhaps not surprising since the basic force balance embodied in (2.5) is valid far beyond its asymptotic regime of applicability.

Our study raises many questions. From an experimental perspective, our analysis suggests ways to probe the rheology of complex fluids since the bending, stretching, falling, and rising responses probe different regimes of fluid behaviour and are translated directly into different shape evolutions. We have ignored the effects of inertia and surface tension, and although they are not important in the phenomena that we consider, much remains to be done on both the theoretical and experimental front to account for their effect in other situations.

We acknowledge the 2003 Summer Program in Geophysical Fluid Dynamics at the Woods Hole Oceanographic Institution, where much of this work was carried out. We thank Jeremy Teichman for the spectral code used herein, Keith Bradley, Jose Bico, Yoel Forterre and Kyung-Ho Roh for help with experiments, and Ronald Larson for useful discussions.

Appendix. Derivation of the equation for the centreline of the filament

In this Appendix we derive (2.5) using standard methods from weakly nonlinear asymptotics (see e.g. Hinch 1991). For small departures from an initial straight line, we scale $y \sim O(\epsilon)$, $t \sim O(\epsilon^2)$, $Wi \sim O(\epsilon^2)$, and $Re \sim O(\epsilon^4)$. Next we expand the velocity, stress, pressure fields, location of the centreline of the sheet H, and its thickness h as series in ϵ, writing

$$u = u_0 + \epsilon^2 u_2 + O(\epsilon^4), \qquad \epsilon v = v_0 + \epsilon^2 v_2 + O(\epsilon^4),$$
$$H = \epsilon H_0 + \epsilon^3 H_2 + O(\epsilon^5), \qquad h = \epsilon h_0 + \epsilon^3 h_2 + O(\epsilon^5),$$

$$p = p_0 + \epsilon^2 p_2 + O(\epsilon^4), \qquad \mathscr{T}^{xx} = \mathscr{T}_0^{xx} + \epsilon^2 \mathscr{T}_2^{xx} + O(\epsilon^4),$$
$$\mathscr{T}^{xy} = \epsilon \mathscr{T}_0^{xy} + \epsilon^3 \mathscr{T}_2^{xy} + O(\epsilon^5), \qquad \mathscr{T}^{yy} = \mathscr{T}_0^{yy} + \epsilon^2 \mathscr{T}_2^{yy} + O(\epsilon^4).$$

Substituting the expansions into (2.1) and (2.2) yields the scaled equation for mass conservation

$$\epsilon^2 u_x + v_y = 0, \tag{A 1}$$

and the equations for conservation of momentum (2.2) in the x- and y-directions are

$$\epsilon^4 Re(u_t + \epsilon^2 u u_x + v u_y) = -\epsilon^2 p_x + \epsilon^2 u_{xx} + u_{yy} + \epsilon^2 \mathscr{T}_x^{xx} + \epsilon^2 \mathscr{T}_y^{xy}, \tag{A 2a}$$
$$\epsilon^4 Re(v_t + \epsilon^2 u v_x + v v_y) = -\epsilon^2 p_y + \epsilon^2 v_{xx} + v_{yy} + \epsilon^4 \mathscr{T}_x^{xy} + \epsilon^2 \mathscr{T}_y^{yy} - \epsilon^4 \varpi. \tag{A 2b}$$

Finally, the constitutive equations (2.3) for the stress components become

$$\mathscr{T}_t^{xx} + \epsilon^2 u \mathscr{T}_x^{xx} + v \mathscr{T}_y^{xx} - 2\epsilon^2 (\mathscr{T}^{xx} u_x + \mathscr{T}^{xy} u_y) = -\frac{1}{Wi}(\mathscr{T}^{xx} - \mathscr{G}), \tag{A 3a}$$

$$\mathscr{T}_t^{yy} + \epsilon^2 u \mathscr{T}_x^{yy} + v \mathscr{T}_y^{yy} - (2\epsilon^2 \mathscr{T}^{xy} v_x + \mathscr{T}^{yy} v_y) = -\frac{1}{Wi}(\mathscr{T}^{yy} - \mathscr{G}), \tag{A 3b}$$

$$\mathscr{T}_t^{xy} + \epsilon^2 u \mathscr{T}_x^{xy} + v \mathscr{T}_y^{xy} - (\mathscr{T}^{xx} v_x + \mathscr{T}^{yy} u_y) = -\frac{1}{Wi} \mathscr{T}^{xy}. \tag{A 3c}$$

The kinematic boundary condition in (2.4) reads

$$v = \left(H \pm \tfrac{1}{2} h\right)_t + \epsilon^2 u \left(H \pm \tfrac{1}{2} h\right)_x, \tag{A 4}$$

and the stress-free condition (2.4b),

$$-\epsilon^2(-p + 2u_x + \mathscr{T}^{xx})\left(H_x \pm \tfrac{1}{2} h_x\right) + (u_y + v_x + \epsilon^2 \mathscr{T}^{xy}) = 0, \tag{A 5a}$$
$$(\epsilon^2(u_y + v_x) + \epsilon^4 \mathscr{T}^{xy})\left(H_x \pm \tfrac{1}{2} h_x\right) - \epsilon^2 p + 2v_y + \epsilon^2 \mathscr{T}^{yy} = 0. \tag{A 5b}$$

At leading order, $O(\epsilon^0)$, the continuity equation (A 1) and the kinematic boundary condition (A 4) are $v_0 = H_{0t}$ and $h_{0t} = 0$, while (A 2a) and the stress-free boundary condition (A 5a) give

$$u_0 = H_{0xt}(H_0 - y) + \overline{u}_0(x), \tag{A 6}$$

with $\overline{u}_0(x)$ the velocity of the centreline of the sheet, i.e. $y = H_0$. Differentiating. (A 6) once with x gives the rate of extensional strain of the centreline, which is the tension, T,

$$T = \overline{u}_{0x} + H_{0x} H_{0xt}. \tag{A 7}$$

For a sheet that is pinned at its ends, horizontal stress balance requires that $T_x = 0$, so that the tension $T = T(t)$. Integrating (A 7) with $x \in [-1/2, 1/2]$, imposing $\overline{u}_0(0, t) = 0$ (from symmetry) and $\overline{u}_0(\pm 1/2, t) = 0$ (no-slip) as boundary conditions, we find that the average tension in the filament is as in (2.6).

Assuming that the flow is purely extensional and homogeneous throughout the sheet, we find $\mathscr{T}_{0y}^{xx} = \mathscr{T}_{0y}^{yy} = \mathscr{T}_{0y}^{xy} = \Psi_x = 0$, where $\Psi = \mathscr{T}^{xx} - \mathscr{T}^{yy}$ is the first normal stress difference. At leading order, the Oldroyd-B equations (A 3) are then

$$\mathscr{T}_{0t}^{xx} = -\frac{1}{Wi}\left(\mathscr{T}_0^{xx} - \mathscr{G}\right), \quad \mathscr{T}_{0t}^{yy} = -\frac{1}{Wi}\left(\mathscr{T}_0^{yy} - \mathscr{G}\right), \tag{A 8a, b}$$

$$\mathscr{T}_{0t}^{xy} = \mathscr{T}_0^{xx} v_{0x} + \mathscr{T}_0^{yy} u_{0y} - \frac{1}{Wi} \mathscr{T}_0^{xy}. \tag{A 8c}$$

Combining (A 8a, b) yields an equation for the evolution of the first normal stress difference $\Psi = \mathscr{T}^{xx} - \mathscr{T}^{yy}$, which when integrated in time is

$$\Psi = \Psi_0 \, \mathrm{e}^{-t/Wi}, \tag{A 9c}$$

where $\Psi(t=0) = \Psi_0$. Thus, at leading order, the first normal stress difference Ψ relaxes to zero, consistent with a relatively small Weissenberg number $Wi \sim O(\epsilon^2)$, whence the strain in the flow is not powerful enough to maintain a non-zero Ψ. Finally, using the continuity equation and the kinematic boundary condition, along with (A 6) and (A 9), in (A 8c) gives us an evolution equation for the elastic shear stress, $\sigma = \mathscr{T}_0^{xy}$, as

$$\sigma_t = \Psi_0 \, \mathrm{e}^{-t/Wi} H_{xt} - \frac{1}{Wi}\sigma \tag{A 10c}$$

where $Wi = \lambda \rho g d/6\mu$ is the appropriate Weissenberg number, with λ the longest relaxation time of the fluid. Integrating (A 10c) with the initial condition $\sigma(x, 0) = 0$ for the case of pure (initial) extension of the sheet, we find $\sigma = \Psi_0 H_x \mathrm{e}^{-t/Wi}$. If the initial thickness of the sheet at leading order is uniform, i.e. $h_{0x} = 0$, then the kinematic boundary condition implies that $h_0 = \text{const.} = d$. With this assumption, $T_x = 0$ at $O(\epsilon^2)$ from the stress-free boundary condition (A 5a), and the leading-order pressure and elastic stress are related by $p_0 - \mathscr{T}_0^{yy} = -2u_{0x}$, with u_{0x} obtained by differentiating (A 6).

Moving now to $O(\epsilon^4)$, we integrate (A 2b) to obtain the equation for pressure at $O(\epsilon^2)$. We use this expression, along with the stress-free boundary condition (A 5a) and (A 5b) at this order, and impose orthogonality of the solution at $O(\epsilon^4)$ to that of the leading-order homogeneous solution. The Fredholm-alternative theorem (Hinch 1991) gives a solvability condition for $H_0(x, t)$, and thus an equation of motion for the centreline of the sheet, (2.5).

REFERENCES

Buckmaster, J. D., Nachman, A. & Ting, L. 1975 The buckling and stretching of a viscida. *J. Fluid Mech.* **69**, 1–20.

Denn, M. M. 2004 Fifty years of non-Newtonian fluid dynamics. *AIChE J.* **50**, 2335–2345.

Entov, V. M. & Hinch, E. J. 1997 Effect of a spectrum of relaxation times on the capillary thinning of a filament of elastic liquid. *J. Non-Newtonian Fluid Mech.* **72**, 31–53.

Entov, V. M. & Yarin, A. L. 1984 The dynamics of thin liquid jets in air. *J. Fluid Mech.* **140**, 91–111.

Hinch, E. J. 1991 *Perturbation Methods*. Cambridge University Press.

Howell, P. D. 1996 Models for thin viscous sheets. *Eur. J. Appl. Maths* **7**, 321–343.

Keiller, R. A. 1992 Extending filaments of an Oldroyd-B fluid. *J. Non-Newtonian Fluid Mech.* **42**, 37–48.

Larson, R. G. 1988 *Constitutive Equations for Polymer Melts and Solutions*. Butterworth.

Larson, R. G. 1999 *Structure and Rheology of Complex Fluids*. Oxford University Press.

McKinley, G. H. & Sridhar, T. 2002 Filament stretching rheometry of complex fluids. *Annu. Rev. Fluid Mech.* **34**, 375–415.

Olagunju, D. O. 1999 A 1-D theory for extensional deformation of a viscoelastic filament under exponential stretching. *J. Non-Newtonian Fluid Mech.* **87**, 27–46.

Oldroyd, J. G. 1950 On the formulation of rheological equations of state. *Proc. R. Soc. Lond.* A **200**, 523–541.

Ribe, N. M. 2001 Bending and stretching of thin viscous sheets. *J. Fluid Mech.* **433**, 135–160.

Teichman, J. & Mahadevan, L. 2003 The viscous catenary. *J. Fluid Mech.* **478**, 71–80.

Trefethen, L. N. 2000 *Spectral Methods in MATLAB*. SIAM.